ACS OMEGA

http://pubs.acs.org/journal/acsodf

Article

Tribology Dependence of Annealed a-C:H Films in Dry Air and Methanol Environments

Zhenguo Lai,[‖] Changning Bai,[‖] Lei Sun, Qian Jia, Kaixiong Gao,* and Bin Zhang*

Cite This: *ACS Omega* 2022, 7, 7472−7480

Read Online

ACCESS | Metrics & More | Article Recommendations

ABSTRACT: In the present study, we obtained a-C:H films with different nanostructures by annealing from room temperature to 400 °C. The influence of the nanostructures on tribological performance in dry air and methanol environments was investigated by a reciprocating tribometer. Our results show that the tribological performance of a-C:H films follows different rules in the two environments. In dry air, tribological properties are controlled by the transfer film and mechanical properties. In methanol, friction and wear are determined by the hydrogen bonding structure, where friction coefficients relate on saturation effects of sp^3-CH, and the wear properties depend on the "collapse effect" that the more the sp^3-CH_3 and sp^3-CH_2, the easier the wear out of bulk a-C:H films. Our work provides guidance for the application of a-C:H films in the methanol environment.

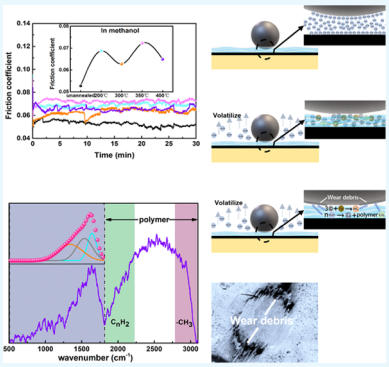

INTRODUCTION

Carbon neutral is one of the hottest topics today for the energy crisis and environmental pollution.[1] According to the International Energy Agency (IEA) report, global fuel vehicles consume 30% of energy, and carbon dioxide (CO_2) emissions are as high as 21%.[2] Consequently, the use of new fuel vehicles, like fuel-cell vehicles, blade electric vehicles, and methanol/fuel hybrid power vehicles, instead of traditional ones, is very important to reduce energy consumption and CO_2 emissions.[3] Today, in China, using methanol as a fuel replacing methanol-gasoline in passenger cars has been put forward. Compared with other vehicles, pure methanol fuel vehicles have the advantages of high power density,[4] low emissions, green cycle,[5] and excellent economy. As shown in Table 1, the economics of different types of vehicles are collected, indicating that methanol vehicles are the most competitive. Nevertheless, the wear of moving mechanics of fuel injectors severely limits and hinders the application of pure methanol fuel vehicles.[6] To avoid this kind of wear from mechanical parts, deposition of thin solid lubricious films onto the surface of the mechanical parts is very useful.

Table 1. Economics of Different Types of Vehicles

	gasoline vehicle	blade electric vehicle	fuel-cell vehicle	methanol vehicle
full-life mileage (10 000 KM)	80−100	45−60	50−100	80−100
core power part cost (RMB)	30 000	170 000	100 000	31 200
energy consumption cost per hundred kilometers (RMB)	57−60	18−20	70−80	35−39
million kilometer consumption (RMB)	600 000	520 000	800 000	381 200
	−630 000	−540 000	−900 000	−421 200

To date, nitride films, carbide films, diamond-like carbon (DLC) films, etc., are widely employed as solid lubricating films. DLC films, composed of sp^2 and sp^3 carbon bonding structures, are in the limelight because of their excellent mechanical hardness, perfect anticorrosion properties, heat conduction, high electrical resistance, etc.[7,8] It is worth noting that the hydrogenated carbon film (a-C:H) has a super-low coefficient of friction (COF < 0.01), which has been extensively studied in recent years. Erdemir et al. developed a high hydrogen content a-C:H film that exhibits super-low friction performance under argon and nitrogen atmospheres, which can be attributed to the low surface energy caused by hydrogen saturation and the charge repulsion-caused polarization.[9−11] However, a-C:H films cannot maintain ultralow friction in the atmospheric environment. Zhang et al. have developed fullerene-like hydrogenated carbon (FL-C:H) films with super-low friction in the atmospheric environment,

Received: September 14, 2021
Accepted: January 21, 2022
Published: February 23, 2022

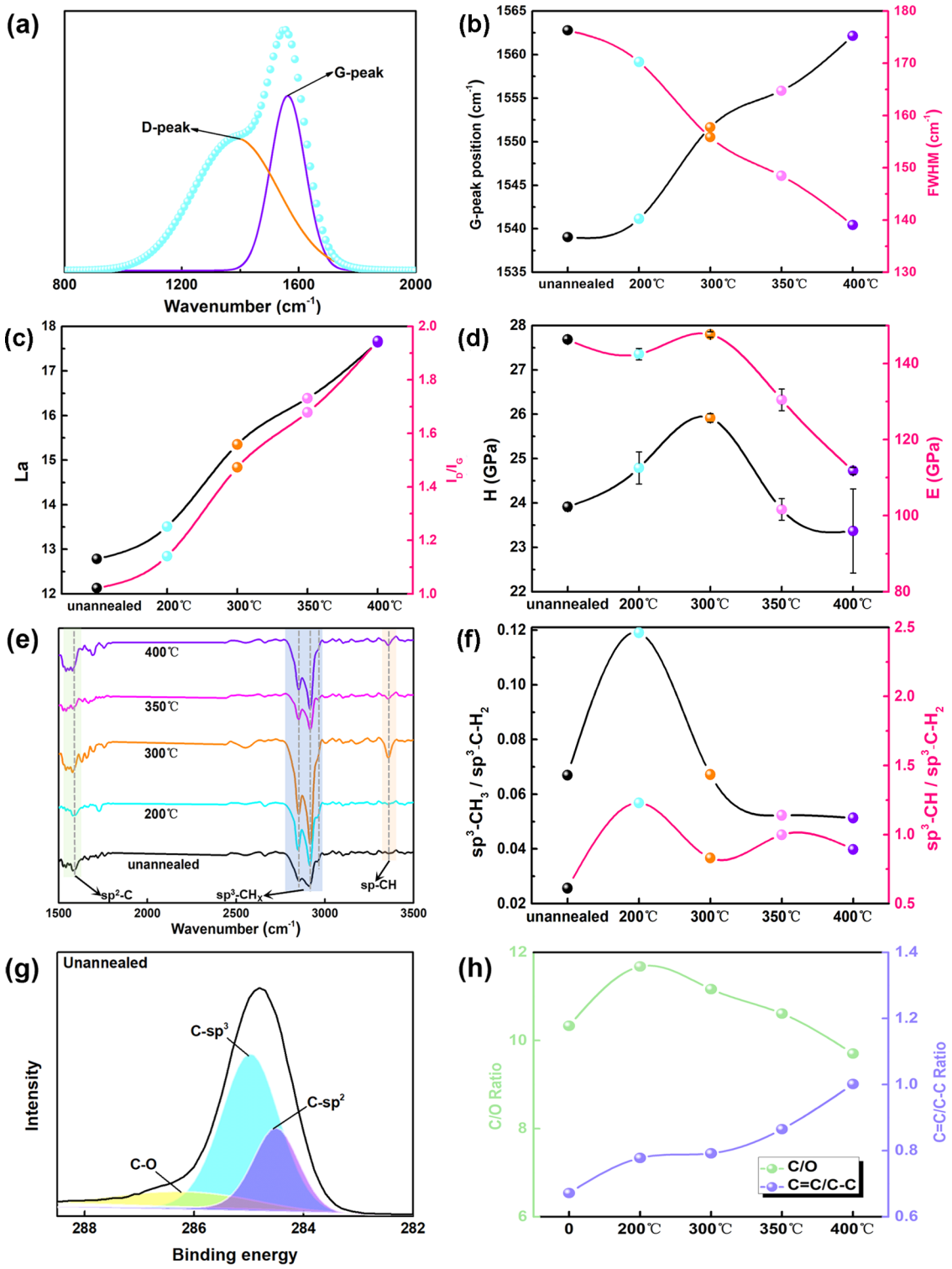

Figure 1. (a) Raman spectrum of the a-C:H film; (b) G-peak position and FWHM; (c) I_D/I_G and L_a; (d) hardness and elastic modulus of films; (e) FTIR analysis results including sp^3-CH_3/sp^3-CH_2 and sp^3-CH/sp^3-CH_2; (f) schematic diagram of XPS spectra by the Gaussian function fitting; (g) C/O and C═C/C−C ratios of films; and (h) FTIR spectra.

attributed to the high hardness and high elasticity induced by fullerene-like structures. Still, the FL-C:H films have a limited lifespan in a vacuum environment.[12−15] Chen et al. revealed that hydrogen-induced diversity in a-C:H:Si film structures, such as polymer-like, diamond-like, or sp^2-bonded a-C, and environmental gas characteristics are the two most influential factors controlling the frictional behaviors of a-C:H:Si films. A suitable hydrogen content range in the film is required to achieve stable super-low friction in a distinct gaseous atmosphere.[16−18] Therefore, inner nanostructure, component, and service environment are the main factors affecting the tribological performance of a-C:H films. The conclusion is also universal in the liquid environment,[19,20] such as vegetable oil-based biolubricants[21] and poly-α olefin oil. Researchers

https://doi.org/10.1021/acsomega.1c05105
ACS Omega 2022, 7, 7472−7480

compared the tribological properties of tetrahedral carbon (ta-C) films and a-C:H films in vegetable oil-based biolubricants and poly-α olefin oil[22,23] and found that the friction coefficient of the ta-C film is generally lower than that of the a-C:H film in the frictional steady state. The wear mechanism of the ta-C film is considered to initiate with a brittle microfracture in the protruding parts, followed by partial spalling with the evolution of the microfracture. The spalled ta-C fragments serve as abrasive particles, significantly increasing the wear of ta-C films.

In comparison, the wear mechanism of the a-C:H film can be ascribed to the graphitization on the topmost surface along with persistent removal of the weakened graphitized layers.[22] Velkavrh also studied the influence of the viscosity of the liquid on the friction properties of a-C:H films and found that the lower the viscosity, the better the tribological performance of a-C:H films. The role of the carbon−hydrogen bond in a-C:H films would make the films possess better tribological properties and better advantage in liquids with lower viscosity.[24]

Thus, as discussed above, it is essential to evaluate the tribology performance of a-C:H films under methanol environments and confirm the tribology dependence on the nanostructure of a-C:H films under methanol environments. In our previous research, it was found that the hydrogen content of a-C:H films ranges only from 24.45 to 23.3% with an increase in the annealing temperature from 25 to 400 °C. Therefore, we can study the influence of the C bonding structure on the tribological behavior through annealing without considering the hydrogen content variation. Hence, in this study, a-C:H films were prepared by PECVD on Si(100) substrates and then annealed at 200, 300, 350, and 400 °C with the protection of argon. The tribological properties and nanostructures of a-C:H films were studied in dry air and methanol. Our study might give guidance for the application of a-C:H films in methanol engines.

EXPERIMENTAL METHODS

Film Preparation. The a-C:H films were deposited by Bipolar Pulsed Plasma Enhanced Chemical Vapor Deposition (BiP-PECVD) on Si(100) substrates in a constant current mode. The Si(100) substrates were ultrasonically cleaned in ethanol for 30 min before putting into the deposition chamber and bombarded to clean impurities and oxides with Ar plasma at a bias voltage of −800 V (current of 0.67) for 20 min when the vacuum was evacuated to 4×10^{-3} Pa. During the deposition, 28 sccm Ar and 14 sccm CH_4 were used as the source gas to fabricate a-C:H films, with a pressure of 6.7 Pa, a bias voltage of −600 V (current of 0.25), and a distance of 50 mm from the surface of the substrates to the upper electrode, respectively.

Characterization Studies. The bonding structures of unannealed and annealed a-C:H films were characterized by Raman spectroscopy (Jobin-Yvon HR-800 with an excitation wavelength of 532 nm), X-ray photoelectron spectroscopy (XPS, PHI5702, America), and Fourier transform infrared (FTIR) spectrometry (Bruker IFS66V, Germany). XPS also gives the film's component and atomic ratio.

The hardness and Young's modulus of unannealed and annealed a-C:H were collected via a nanoindenter (Hysitron Ti950, America) with a constant depth of 70 nm.

Friction Tests. The friction behaviors were tested via a ball-on-disc reciprocating tribometer (MFT-R4000, Lanzhou Huahui Instrument Technology Co., Ltd.). For the friction test, 440c steel balls (φ = 5 mm, R_a = 0.1 nm) against a-C:H films were used as friction pairs with a reciprocating speed of 50 mm/s, load of 10 N, and reciprocating length of 5 mm, which were performed in dry air (∼7.5% relative humidity) and methanol (∼99.9%) environment.

Wear tracks on a-C:H films were explored by a MAX 3D three-dimensional surface profiler (ADE, America), and the wear rates were calculated from the results of wear track analysis by the following equation[17]

$$W = \frac{V}{F_N \times L} \tag{1}$$

where V is the wear volume (mm^3), F_N represents the normal load (N), and L is the reciprocating length (m).

Wear scars on the steel balls were observed on a scanning electron microscope (SEM, Thermo Scientific, Talos 200s, America), and the wear volumes of wear spots were calculated from the diameter of the wear scars by the equation

$$V = \frac{\pi}{6}\left(r - \sqrt{r^2 - \frac{d^2}{4}}\right)\left(\frac{3d^2}{4} + r^2 - \frac{d^2}{4}\right) \tag{2}$$

where d is the wear scar diameter and r is (= 5 mm) the radius of the 440c steel ball.

RESULTS AND DISCUSSION

Structural Characterization and Mechanical Properties of a-C:H Films. Raman spectroscopy is a fast and nondestructive method for the characterization of carbon materials.[25,26] The original Raman spectra of unannealed and annealed a-C:H films are fitted by a Gaussian function (Figure 1a), and the results are described in Figure 1b,c. With the increase in the annealing temperature, it could be observed that the G-peak blue shift and I_D/I_G increase (G-position: from 1538 to 1562 cm^{-1}, I_D/I_G: from 1.0213 to 1.9453), while the full width at half-maximum (FWHM) of G-peak reduces. Thus, it can be speculated that the order degree of a-C:H films' structure has improved. The result of the H content is calculated by the following equation[27]

$$H_{atom}[\text{atom }\%] = 21.7 + 16.6\ \log\{m/I_G[\mu m]\} \tag{3}$$

where m is the slope of the Raman spectrum. The H_{atom} content of the a-C:H film ranges from 21−23 atom %, which is in accordance with our previous reports.[28] Thus, in the present study, it can be assured that annealing has a negligible impact on the desorption of H_{atom}. In addition, the sp^2 carbon cluster size (L_a) could be calculated by the following formula

$$\frac{I_D}{I_G} = C'(\lambda){L_a}^2 \tag{4}$$

where $C'(532)$ = 0.00625 when λ = 532 nm.[26] The calculated result of L_a is shown in Figure 1c, which linearly increased with the annealing temperature.

The variation of nanohardness (H), shown in Figure 1d, indicates an inverted "V" change where the maximum value turns out at 300 °C, while the elastic modulus (E) first remains at a certain level and then decreases linearly beyond 300 °C. However, it is different from the previous reported works in which the increase in the annealing temperature leads to the decrease in both hardness and Young's modulus of a-C:H films.[12,33−36]

https://doi.org/10.1021/acsomega.1c05105
ACS Omega 2022, 7, 7472−7480

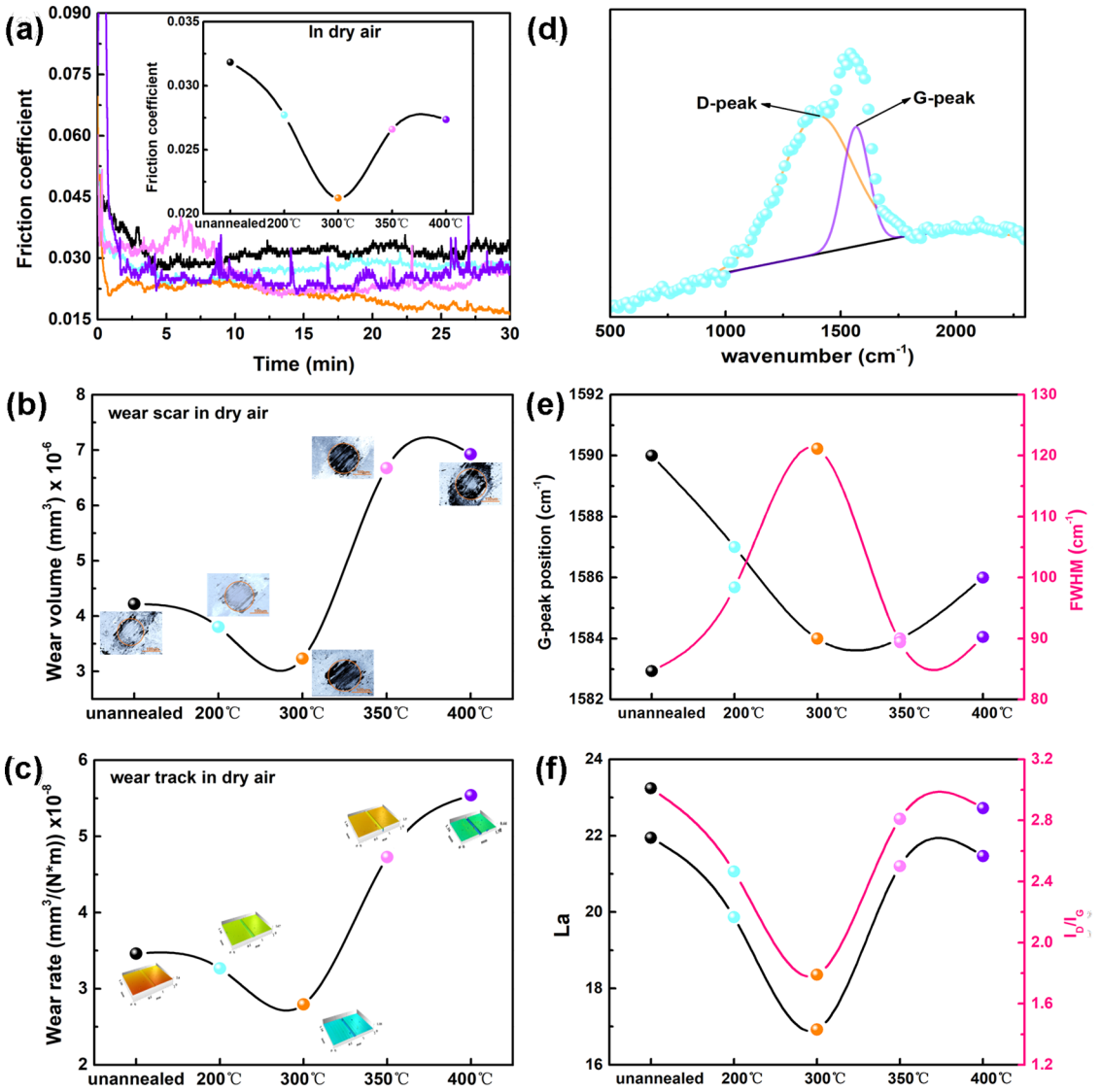

Figure 2. (a) Friction coefficient and average friction coefficient of a-C:H films in dry air; (b) SEM images and wear volume; (c) three-dimensional contour maps and wear rates; (d) Raman spectra of wear scars; (e) G-peak position and FWHM; and (f) I_D/I_G and L_a.

The chemical state of a-C:H films is monitored by Fourier transform infrared spectroscopy (FTIR), as shown in Figure 1e; it shows that sp^3-CH_X has a broad bump between 2750 and 2980 cm^{-1}, which contains three peaks corresponding to asymmetric sp^3-CH at 2920 cm^{-1}, asymmetric sp^3-CH_3 at 2960 cm^{-1}, and sp^3-CH_2 at 2850 cm^{-1}.[29] Meanwhile, a peak at ~3300 cm^{-1} is attributed to the sp-CH species.[30] A broad band at 1650 cm^{-1} is attributed to the sp^2-C species.[31] In addition, the bump of 2700 to 3000 cm^{-1} were fitted with Gauss function corresponding to asymmetric sp^3-CH at 2920 cm^{-1}, asymmetric sp^3-CH_3 at 2960 cm^{-1}, and sp^3-CH_2 at 2850 cm^{-1}, respectively. The variation ratio of sp^3-CH_3/sp^3-CH_2 is shown in Figure 1f, indicating that the relative ratio of breaking of C−H increases with the temperature increasing to 200 °C and then decreases to a certain level beyond 350 °C. Considering the negligible change of the H_{atom} content in a-C:H films, one can speculate that the H bonding to sp^3-CH_3 site transforms into sp^3-$CH_{x(1-2)}$. To assure this speculation, the ratio of sp^3-CH/sp^3-CH_2 shows nearly the same trend as that of sp^3-CH_3/sp^3-CH_2 in Figure 1f, where, as the temperature increases to 200 °C, an inflection point appears and then stabilizes, indicating that both sp^3-CH_3 and sp^3-CH are dominating when the annealed temperature is below 200 °C, and the breaking of sp^3-CH_3 and the forming of sp^3-CH slowed down beyond 350 °C.

X-ray photoelectron spectroscopy (XPS) spectra were used to obtain the chemical bonding information and element content of a-C:H films. As shown in Figure 1g, the C 1s spectra of a-C:H films could be divided into three peaks with the Gaussian function, peaks located at 286.2, 285.2, and 284.5 eV, representing C−O, C-sp^3, and C-sp^2, respectively.[32] As shown in Figure 1h, the ratio of C═C/C−C increases with the increase in the annealing temperature, while the C/O ratio increases when the annealing temperature reaches 200 °C and then decreases with the annealing temperature at 400 °C. It should be noted that during the deposition process, there was no oxygen. Thus, the presence of oxygen can be attributed to contamination during the storage and transfer; hence the more the oxygen, the higher the porosity in the a-C:H films.

Frictional Properties of a-C:H Films in Dry Air. The friction coefficient in dry air is shown in Figure 2a, which indicates an inverted variation compared to H, indicating a "V"

https://doi.org/10.1021/acsomega.1c05105
ACS Omega 2022, 7, 7472−7480

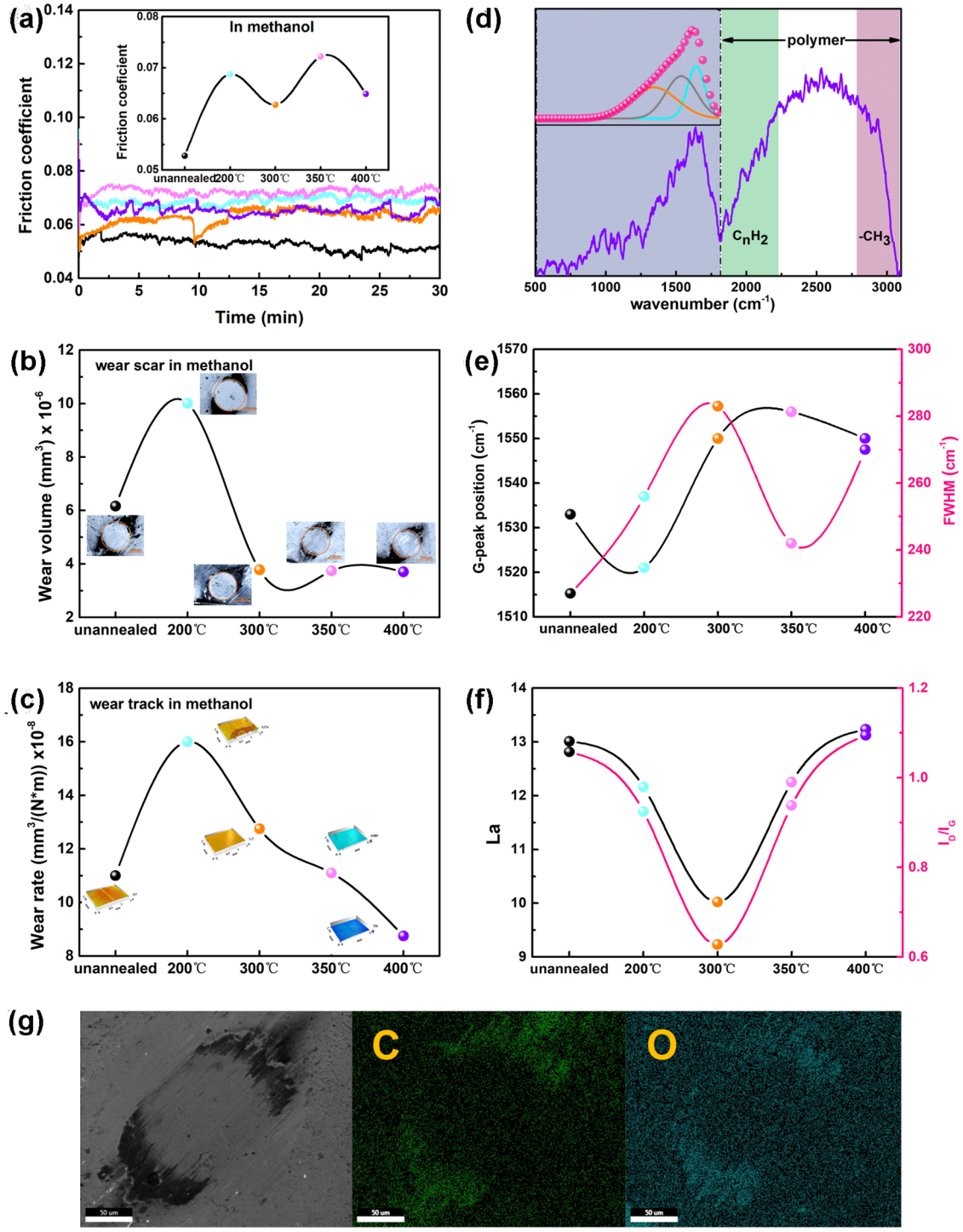

Figure 3. (a) Friction coefficient and average friction coefficient of a-C:H films in methanol environment; (b) SEM images and wear volumes; (c) three-dimensional contour maps and wear rates; (d) Raman spectra of wear debris; (e) G-peak position and FWHM; (f) I_D/I_G and L_a; and (g) SEM element mapping image of wear debris.

change. It can be seen that the unannealed a-C:H film has the highest friction coefficient of 0.032, and the a-C:H film annealed at 300 °C shows the lowest friction coefficient of 0.021. The corresponding wear volumes of 440c steel balls and SEM images of wear scars are shown in Figure 2b, and the wear rates of a-C:H films and the corresponding three-dimensional profile images of wear tracks are described in Figure 2c. Both the wear rate and wear volume have the same trend as that of the friction coefficient.

Interestingly, the wear volume of the friction pairs depends on the hardness of a-C:H films; the greater the hardness of a-C:H films, the lesser the wear of the friction pairs and vice versa. However, the friction coefficient is not only controlled by H of a-C:H films but also the nanostructure evolution of the sliding interface.[37,38] Thus, Raman spectra were collected from the wear scars of 440c steel balls, as shown in Figure 2d. Interestingly, though the G-peak position, FWHM, I_D/I_G, and L_a show a regularity as shown in Figure 2e,f, Raman signals of

https://doi.org/10.1021/acsomega.1c05105
ACS Omega 2022, 7, 7472−7480

transfer films on wear scars differ with a-C:H films themselves. The G-peak position, I_D/I_G, and L_a give the "V" change, and FWHM shows an inverted "V" change, in accordance almost well with the friction coefficient. Therefore, it is concluded that the frictional properties are not only dependent on the hardness but also on the nanostructure variation of the contact interface of the a-C:H film.

Frictional Properties of a-C:H Films in Methanol. The friction coefficient of a-C:H films in methanol is shown in Figure 3a, indicating an inverted "W," which appears to be of the same order with that in dry air. The unannealed a-C:H film has the lowest friction coefficient of 0.052. The friction coefficients of annealed a-C:H films at corresponding temperatures are 0.069 (200 °C), 0.061 (300 °C), 0.071 (350 °C), and 0.065 (350 °C).

The corresponding wear volumes of 440c steel balls and SEM images of wear scars are shown in Figure 3b, and the wear rates of a-C:H films and three-dimensional profile images of wear tracks are described in Figure 3c. From the SEM images, it can be clearly observed that the wear debris scatters around the wear scars of 440c steel balls. The wear volume increases with the increase in temperature up to 200 °C and then decreases to a certain level at temperatures 300, 350, and 400 °C, as shown in Figure 3b, which is different from the conditions of dry air and it is not dependent on the H of the film. The wear rate of a-C:H films increases with the temperature increasing to 200 °C and then decreases almost linearly beyond the temperature of 200 °C, the same as that of the wear volume of wear scars of 440c steel balls. Thus, it is assured that methanol has an important influence on the tribology of a-C:H films.

To fully understand why the wear behavior was abnormal, the wear debris on the 440c steel ball was investigated. Figure 3d shows the Raman spectra of the wear debris in methanol at 500−3500 cm^{-1}. There are two broad peaks at about 1000−1800 cm^{-1} divided into three peaks, roughly located at 1366, 1550, and 1680 cm^{-1}, corresponding to peak D, peak G, and C═O vibrations.[39] The big bump, around 1800−3050 cm^{-1} can be observed. Tabata et al. found that the Raman spectroscopy of C_nH_2 with different chain lengths is distributed between 1880 and 2200 cm^{-1}.[40] Rabia et al. believe that the peak between 1800 and 2400 cm^{-1} is related to sp-C.[41] Cataldo et al. recorded the Raman spectrum of the polyene with a weak band at 2230 cm^{-1}.[42] Other research studies showed that two bands centered at 2950 and 2840 cm^{-1} (CH_3 asymmetric and symmetric stretching vibrations) dominate the stimulated Raman spectrum of methanol.[43,44] Considering all of the above, we can speculate that there are various polymers produced from the friction process in the methanol environment. As reported before, the G-peak position, I_D/I_G, and L_a show the same trend, and FWHM is the opposite of these three.[45] However, we found that these four indicators are not in this manner in our analysis of wear debris in methanol. The phenomenon is due to the influence of the polymer-like structure of wear debris, endowing the Raman signal with a high fluorescence background, which makes the Raman analysis of wear debris in a methanol environment meaningless. To indirectly verify the polymer statement, we perform a SEM element mapping scan on the wear scars, shown in Figure 3g, and find that C and O are obviously accumulated in the place of the wear debris.

Furthermore, the FTIR data between 2750 and 2980 cm^{-1}, deconvoluted into three peaks and corresponding to asymmetric sp^3-CH at 2920 cm^{-1}, asymmetric sp^3-CH_3 at 2960 cm^{-1}, and sp^3-CH_2 at 2850 cm^{-1}[29] are summarized in Table 2. It is evident that the result of friction coefficients is

Table 2. Proportion Economics of Different Types of Vehicles

	100 °C (%)	200 °C (%)	300 °C (%)	350 °C (%)	400 °C (%)
sp^3-CH	59.58	42.59	52.7	48.77	51.45
sp^3-CH_2	36.43	52.34	43.76	48.68	45.91
sp^3-CH_3	3.99	5.07	3.54	2.55	2.64

consistent mainly with sp^3-CH/sp^3-CH_2 ratios of a-C:H films (the higher the ratio of sp^3-CH/sp^3-CH_2, the higher the friction coefficient), but the wear rates of a-C:H films and wear volumes of 440c steel balls are affected by sp^3-CH_3/sp^3-CH_2 (the higher the ratio of sp^3-CH/sp^3-CH_2, the higher the wear rate and volume). The proportion of different bonding sp^3-CH_x is described in Table 2. It should be noted that in the present work, the H_{atom} before and after annealing is mostly constant, and more sp^3-CH means few dangling bonds, which is favorable for low friction and wear. For wear properties, there is another reason for different variations from that of the friction coefficients. From the perspective of bond energy (high to low) in a-C:H films, they are C−H (bond energy 285.3−285.4 eV) and C═C (bond energy 284.2−284.3 eV).[46] Thus, it can be speculated that the breaking of C═C is easier than C−H, and methanol molecules have different passivation effects on the surface of the carbon film, like water molecules,[47] where a hydrogen bond interacts between hydroxyl groups in methanol and −CH on the surface of a-C:H films. The interacting force of different bonding sites is in a sequence of sp^3-CH_3, sp^3-CH_2, and sp^3-CH. The higher the interacting force, the easier the breaking of sp^3-C by breaking the bond of C═C to wear out of bulk a-C:H films, and we call it the "collapse effect."

Comparison and the Mechanism of Frictional Properties in Both Environments. It is evident that the friction coefficient and wear rate of a-C:H films have no uniform trends with the annealing temperature in dry air and methanol environments.

Comparing the SEM images of both environments, it is noted that there is a transfer film under a dry environment (Figure 2b), and the transfer film disappears in the methanol environment after rubbing (Figure 3b). The disappearance of the transfer films in methanol is attributed to the polarity and low viscosity of the methanol liquid. This phenomenon is the main factor that causes more reduction in the friction coefficient in the methanol environment than in dry air, as shown in Figures 2a and 3a. However, the wear rate of a-C:H films in methanol is lower than that in dry air, which is a characteristic of liquid lubrication. According to the friction process of a-C:H films in dry air and methanol environments, the friction mechanism diagrams are shown in Figure 4a,b. According to the transfer film theory,[48] the a-C:H film first contacts the friction pair under dry air.

During the reciprocating friction process, a stable layer of transfer film is formed on the surface of the friction pair after a running period, and abraded nanoirons induced the growth of graphite-like structures, which can be seen from HRTEM images in Figure 4a.

https://doi.org/10.1021/acsomega.1c05105
ACS Omega 2022, 7, 7472−7480

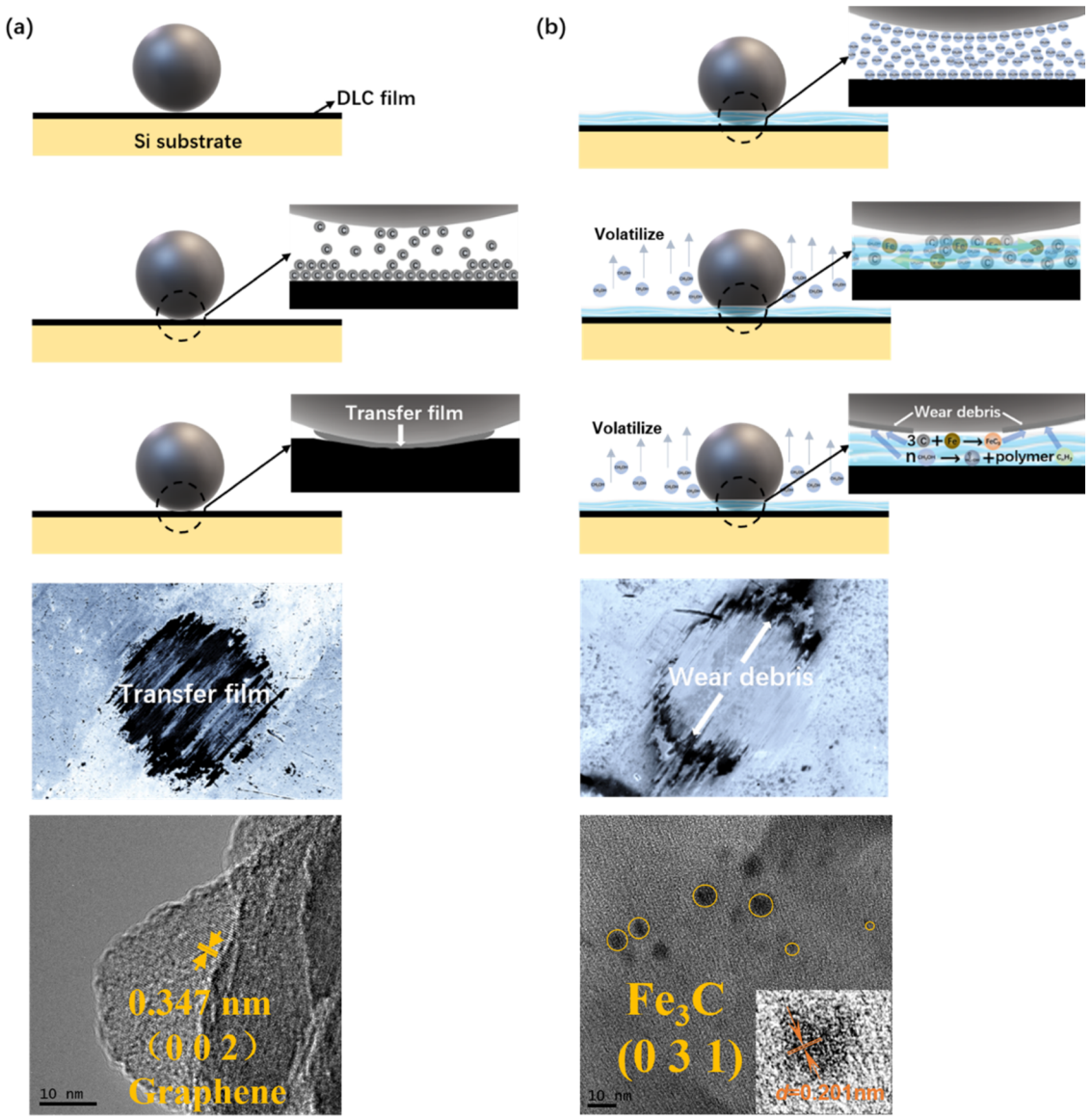

Figure 4. (a) Friction mechanism diagram and TEM in dry air and (b) friction mechanism diagram and TEM in the methanol environment.

During the reciprocating friction process, after a short running, a stable transfer film is formed on the surface of the friction pair, the worn nanoiron induces the growth of the graphite-like structure, and the degree of graphitization guides the friction coefficient, as can be seen from the HRTEM image in Figure 4a. In the methanol environment, first, the a-C:H film contacts the friction counterpart, and then the methanol liquid fills the contact gap. Here, the friction coefficient is related to the saturation of the a-C:H surface; the more the sp^3-CH, the lower the friction coefficient. The collapse effect guides the wear rate; the more the sp^3-CH_3 and sp^3-CH_2, the easier the a-C:H film is to wear.

Due to the catalytic effects of nanoirons, induced methanol reacts with a fragment of a-C:H to form polymer-like structures, shown in Figure 4b. In addition, the wear debris cannot be adsorbed on the surface of the friction pair due to the continuous flow of the methanol liquid, which is pushed to accumulate around the wear spots.

CONCLUSIONS

We here presented the experimental research on the tribology dependence of annealed a-C:H films in dry air and methanol environments with comparison.

In dry air, the friction coefficient and wear rate of a-C:H films show "V" trends; the lowest friction coefficient, wear rate, and wear volumes are found at 300 °C. The friction coefficient is between 0.021 and 0.032 in our study and the wear rate and wear volume are in the range of 3.2−7.6 ($mm^3/(N{\cdot}m) \times 10^{-8}$) and 2.7−5.6 ($mm^3 \times 10^{-8}$), respectively. In dry air conditions, the friction coefficient is guided by the graphitization of wear debris, and the wear properties for both 440c steel balls and a-C:H films are determined by the hardness of a-C:H films. In the methanol environment, the friction coefficient is between 0.053 and 0.071, and the wear rate and wear volumes are in the range of 3.6−10.0 ($\times mm^3/(N{\cdot}m) \times 10^{-8}$) and 8.7−16.0 ($mm^3 \times 10^{-6}$), respectively, higher than that under dry air. The friction coefficient is related to saturation of the a-C:H surface, i.e., the more the sp^3-CH, the lower the friction coefficient. Moreover, the wear rate is guided by the collapse effect, and

https://doi.org/10.1021/acsomega.1c05105
ACS Omega 2022, 7, 7472−7480

the more the sp^3-CH_3 and sp^3-CH_2, the easier the wear out of the bulk of a-C:H films. It is concluded that the tribology of a-C:H films is dependent on the nanostructure and bonding topology of the film. This study therefore indicates that the a-C:H films can possibly be a practical route to control wear in methanol engines.

AUTHOR INFORMATION

Corresponding Authors

Kaixiong Gao − *State Key Laboratory of Solid Lubrication, Lanzhou Institute of Chemical Physics, Chinese Academy of Sciences, Lanzhou 730000, China*; Email: kxgao@licp.cas.cn

Bin Zhang − *State Key Laboratory of Solid Lubrication, Lanzhou Institute of Chemical Physics, Chinese Academy of Sciences, Lanzhou 730000, China; Center of Materials Science and Optoelectronics Engineering, University of Chinese Academy of Sciences, Beijing 100049, China; Dalian National Laboratory for Clean Energy, Chinese Academy of Sciences, Dalian 116000, China;* orcid.org/0000-0002-9038-7514; Email: bzhang@licp.cas.cn

Authors

Zhenguo Lai − *State Key Laboratory of Solid Lubrication, Lanzhou Institute of Chemical Physics, Chinese Academy of Sciences, Lanzhou 730000, China; Center of Materials Science and Optoelectronics Engineering, University of Chinese Academy of Sciences, Beijing 100049, China*

Changning Bai − *State Key Laboratory of Solid Lubrication, Lanzhou Institute of Chemical Physics, Chinese Academy of Sciences, Lanzhou 730000, China; Center of Materials Science and Optoelectronics Engineering, University of Chinese Academy of Sciences, Beijing 100049, China*

Lei Sun − *State Key Laboratory of Solid Lubrication, Lanzhou Institute of Chemical Physics, Chinese Academy of Sciences, Lanzhou 730000, China; Center of Materials Science and Optoelectronics Engineering, University of Chinese Academy of Sciences, Beijing 100049, China*

Qian Jia − *State Key Laboratory of Solid Lubrication, Lanzhou Institute of Chemical Physics, Chinese Academy of Sciences, Lanzhou 730000, China; Center of Materials Science and Optoelectronics Engineering, University of Chinese Academy of Sciences, Beijing 100049, China*

Complete contact information is available at: https://pubs.acs.org/10.1021/acsomega.1c05105

Author Contributions

[‖]Z.L. and C.B. contributed equally to this work. B.Z. and K.G.: conceptualization, methodology, reviewing, supervision; Z.L.: formal analysis, software, visualization, writing—original draft preparation; C.B.: software, writing—original draft preparation; L.S.: data curation; Q.J.: software.

Notes

The authors declare no competing financial interest.

ACKNOWLEDGMENTS

The authors are grateful for the financial support by the National Key Research and Development Program of China (No. 2020YFA0711002), the Youth Innovation Promotion Association CAS (No. 2017459), and the National Natural Science Foundation of China (No. 52005485).

REFERENCES

(1) Service, R. F. Service Clean Revolution. *Science* **2015**, 1020−1023.

(2) Holmberg, K.; Erdemir, A. The Impact of Tribology on Energy Use And CO_2 Emission Globally and In Combustion Engine And Electric Cars. *Tribol. Int.* **2019**, *135*, 389−396.

(3) Yuan, X.; Liu, X.; Zuo, J. The Development of New Energy Vehicles for A Sustainable Future: A Review. *Renewable Sustainable Energy Rev.* **2015**, *42*, 298−305.

(4) Black, F. M. Overview of The Technical Implications of Methanol and Ethanol as Highway Motor-Vehicle Fuels. *SAE Trans.* **1991**, 1160−1190.

(5) Wang, J.; Tang, C.; Li, G.; Han, Z.; Li, C.; et al. High-Performance MaZrOx (Ma = Cd, Ga) Solid-Solution Catalysts for CO_2 Hydrogenation to Methanol. *ACS Catal.* **2019**, *9*, 10253−10259.

(6) Lyons, J. S. Selection of Ceramics for Methanol Fuel Injector Plungers Based on Tribological Characteristics When Coupled with 4140 Steel. *Mater. Des.* **1998**, *19*, 19−27.

(7) Holland, L.; Ojha, S. M. Deposition of Hard and Insulating Carbonaceous Films on An R.F. Target in A Butane Plasma. *Thin Solid Films* **1976**, *38*, L17−L19.

(8) Spencer, E. G.; Schmidt, P. H.; Joy, D. C.; Sansalone, F. J. Ion-beam-deposited Polycrystalline Diamondlike Films. *Appl. Phys. Lett.* **1976**, *29*, 118−120.

(9) Wang, J.; Li, X.; Wu, G.; Lu, Z.; Zhang, G.; Xue, Q. Origin of Low Friction for Amorphous Carbon Films with Different Hydrogen Content in Nitrogen Atmosphere. *Tribol. Int.* **2019**, *140*, No. 105853.

(10) Liu, S.; Zhang, C.; Osman, E.; Chen, X.; Ma, T.; Hu, Y.; Luo, J.; Ali, E. Influence of Tribofilm on Superlubricity of Highly-hydrogenated Amorphous Carbon Films in Inert Gaseous Environments. *Sci. China: Technol. Sci.* **2016**, *59*, 1795−1830.

(11) Johnson, J. A.; Woodford, J. B.; Chen, X.; Andersson, J.; Erdemir, A.; Fenske, G. R. Insights into "near-frictionless carbon films". *J. Appl. Phys.* **2004**, *95* (12), 7765−7771.

(12) Wang, Z.; Gong, Z.; Zhang, B.; Wang, Y.; Gao, K.; Zhang, J.; Liu, G. Heating Induced Nanostructure and Superlubricity Evolution of Fullerene-like Hydrogenated Carbon Films. *Solid State Sci.* **2019**, *90*, 29−33.

(13) Liu, Y.; Chen, L.; Zhang, B.; Cao, Z.; Shi, P.; Peng, Y.; Zhou, N.; Zhang, J.; Qian, L. Key Role of Transfer Layer in Load Dependence of Friction on Hydrogenated Diamond-like Carbon Films in Humid Air and Vacuum. *Materials* **2019**, *12*, No. 1550.

(14) Wang, C.; Yang, S.; Wang, Q.; Wang, Z.; Zhang, J. Super-Low Friction and Super-Elastic Hydrogenated Carbon Films Originated from a Unique Fullerene-Like Nanostructure. *Nanotechnology* **2008**, *19*, No. 225709.

(15) Wang, Q.; Wang, C.; Wang, Z.; Zhang, J.; He, D. Fullerene Nanostructure-Induced Excellent Mechanical Properties in Hydrogenated Amorphous Carbon. *Appl. Phys. Lett.* **2007**, *91*, No. 141902.

(16) Chen, X.; Kato, T.; Nosaka, M. Origin of Superlubricity in a-C:H:Si Films: A Relation to Film Bonding Structure and Environmental Molecular Characteristic. *ACS Appl. Mater. Interfaces* **2014**, *6*, 13389−13405.

(17) Wang, K.; Yang, B.; Zhang, B.; Bai, C.; Mou, Z.; Gao, K.; Yushkov, G.; Oks, E. Modification of a-C:H Films via Nitrogen and Silicon Doping: the Way to the Superlubricity in Moisture Atmosphere. *Diamond Relat. Mater.* **2020**, *107*, No. 107873.

(18) Shi, J.; Wang, Y.; Gong, Z.; Zhang, B.; Wang, C.; Zhang, J. Nanocrystalline Graphite Formed at Fullerene-Like Carbon Film Frictional Interface. *Adv. Mater. Interfaces* **2017**, *4*, No. 1601113.

(19) Vengudusamy, B.; Mufti, R. A.; Lamb, G. D.; Green, J. H.; Spikes, H. A. Friction Properties of DLC/DLC Contacts in Base Oil. *Tribol. Int.* **2011**, *44*, 922−932.

(20) Broda, M.; Bethke, R. Friction Behavior of Different DLC Coatings by Using Various Kinds of Oil. *SAE Int. J. Mater. Manf.* **2009**, *1*, 832−840.

(21) Hanif, M. T.; Zahid, R.; Mufti, R.; Waqas, M.; Naveed, T. A Review on Tribological Study of DLC Coatings in Combination with Bio Based Lubricants. *Int. J. Mater. Sci. Appl.* **2021**, *10*, 61.

(22) Mobarak, H.; Masjuki, H. H.; Mohamad, E. N.; Kalam, M. A.; Rashedul, H. K.; Rashed, M.; Habibullah, M. Tribological Properties of Amorphous Hydrogenated (a-C:H) and Hydrogen-Free Tetrahedral (ta-C) Diamond-Like Carbon Coatings under Jatropha Biodegradable Lubricating Oil at Different Temperatures. *Appl. Surf. Sci.* **2014**, *317*, 581−592.
(23) Li, X.; Deng, X.; Kousaka, H.; Umehara, N. Comparative Study on Effects of Load and Sliding Distance on Amorphous Hydrogenated Carbon (a-C:H) Coating and Tetrahedral Amorphous Carbon (Ta-C) Coating Under Base-Oil Lubrication Condition. *Wear* **2017**, *392*−*393*, 84−92.
(24) Velkavrh, I.; Kalin, M. Comparison of the Effects of the Lubricant-molecule Chain Length and the Viscosity on the Friction and Wear of Diamond-like-carbon Coatings and Steel. *Tribol. Int.* **2012**, *50*, 57−65.
(25) Ferrari Carlo, A. Determination of Bonding in Diamond-like Carbon by Raman Spectroscopy. *Diamond Relat. Mater.* **2002**, *11*, 1053−1061.
(26) Ferrari, A. C.; Robertson, J. Interpretation of Raman Spectra of Disordered and Amorphous Carbon. *Phys. Rev. B* **2000**, *61*, 14095−14107.
(27) Casiraghi, C.; Ferrari, A. C.; Robertson, J. Raman spectroscopy of hydrogenated amorphous Carbons. *Phys. Rev. B: Condens. Matter Mater. Phys.* **2005**, *72*, No. 85401.
(28) Wang, Z.; Gao, K.; Zhang, B.; Gong, Z.; Wei, X.; Zhang, J. Verification Study of Nanostructure Evolution with Heating Treatment between Thin and Thick Fullerene-Like Hydrogen Carbon Films. *Coatings* **2019**, *9*, No. 82.
(29) Xiao, Y. Q.; Tan, X. Y.; Jiang, L. H.; Xiao, T.; Xiang, P.; Yan, W. S. The Effect Of Radio Frequency Power on the Structural and Optical Properties of a-C:H Films Prepared by PECVD. *J. Mater. Res.* **2017**, *32*, 1231−1238.
(30) Choi, J.; Lee, S. K.; Yoon, C. J.; Oh, S. E.; Lee, C. H. Durability Evaluation of DLC coating through the Enhanced Environmental Tests. In *Optical Materials and Biomaterials in Security and Defence Systems Technology IX, International Society for Optics and Photonics*, Proceedings of SPIE8548, Edinburgh, United Kingdom, November 8, 2012;Zamboni, R.; Kajzar, F.; Szep, A. A., Eds.; SPIE Publishers, 2012; Vol. *8545*.
(31) Semenenko, M.; Okrepka, G.; Yilmazoglu, O.; Hartnagel, H.; Pavlidis, D. Electrical Conditioning of Diamond-Like Carbon Films for the Formation of Coated Field Emission Cathodes. *Appl. Surf. Sci.* **2010**, *257*, 388−392.
(32) Li, R.; Wang, Y.; Zhang, J.; Zhang, J. Origin of Higher Graphitization under Higher Humidity on the Frictional Surface of Self-Mated Hydrogenated Carbon Films. *Appl. Surf. Sci.* **2019**, *494*, 452−457.
(33) Michler, J.; Tobler, M.; Blank, E. Thermal Annealing Behaviour of Alloyed DLC Films on Steel: Determination and Modelling of Mechanical Properties. *Diamond Relat. Mater.* **1999**, *8*, 510−516.
(34) Wong, P. L.; He, F.; Zhou, X. Interpretation of The Hardness of Worn DLC Particles Using Micro-Raman Spectroscopy. *Tribol. Int.* **2010**, *43*, 1806−1810.
(35) Takadoum, J.; Rauch, J. Y.; Cattenot, J. M.; Martin, N. Comparative Study of Mechanical and Tribological Properties of CNX and DLC Films Deposited by PECVD Technique. *Surf. Coat. Technol.* **2003**, *174*−*175*, 427−433.
(36) Wang, L.; Nie, X.; Xin, H. Effect of Thermal Annealing on Tribological and Corrosion Properties of DLC Coatings. *J. Mater. Eng. Perform.* **2013**, *22*, 3093−3110.
(37) Ma, T. B.; Hu, Y. Z.; Wang, H. Molecular Dynamics Simulation of Shear-Induced Graphitization of Amorphous Carbon Films. *Carbon* **2009**, *47*, 1953−1957.
(38) Dwivedi, N.; Yeo, R. J.; Zhang, Z.; Dhand, C.; Tripathy, S.; Bhatia, C. S. Interface Engineering and Controlling the Friction and Wear of Ultrathin Carbon Films: High sp^3 Versus High sp^2 Carbons. *Adv. Funct. Mater.* **2016**, *26*, 1526−1542.
(39) Schneider, S. H.; Boxer, S. G.; et al. Vibrational Stark Effects of Carbonyl Probes Applied to Re-interpret IR and Raman Data for Enzyme Inhibitors in Terms of Electric Fields at the Active Site. *J. Phys. Chem. B* **2016**, *120*, 9672.
(40) Tabata, H.; Fujii, M.; Hayashi, S.; Doi, T.; Wakabayashi, T. Raman and Surface-Enhanced Raman Scattering of a Series of Size-Separated Polyynes. *Carbon* **2006**, *44*, 3168−3176.
(41) Rabia, A.; Tumino, F.; Milani, A.; Russo, V.; Casari, C. S.; et al. Scanning Tunneling Microscopy and Raman Spectroscopy of Polymeric $sp-sp^2$ Carbon Atomic Wires Synthesized on the Au(111) Surface. *Nanoscale* **2019**, *11*, 18191−18200.
(42) Cataldo, F. The Role of Raman Spectroscopy in the Research on sp-Hybridized Carbon Chains: Carbynoid Structures Polyynes and Metal Polyynides. *J. Raman Spectrosc.* **2008**, *39*, 169−176.
(43) Nixdorf, J.; Di Florio, G.; Brockers, L.; Borbeck, C.; Hermes, H.; Egelhaaf, S.; Gilch, P. Uptake of Methanol by Poly(methyl methacrylate): An Old Problem Addressed by a Novel Raman Technique. *Macromolecules* **2019**, *52*, 4997−5005.
(44) Emin, A.; Hushur, A.; Mamtimin, T. Raman Study of Mixed Solutions of Methanol and Ethanol. *AIP Adv.* **2020**, *10*, No. 065330.
(45) Donnet, C.; Erdemir, A. *Tribology of Diamond-like Carbon Films: Fundamentals and Applications*; Springer: USA, 2007.
(46) Nitta, Y.; Okamoto, K.; Nakatani, T.; Shinohara, M. Effect of the Surface Bond States in As-Deposited DLC Films on the Incorporation of Nitrogen and Oxygen Atoms. *IEEE Trans. Plasma Sci.* **2012**, *40*, 2073−2078.
(47) Liu, S. W.; Zhang, C. H.; Osman, E.; Chen, X. C.; Ma, T. B.; Hu, Y. Z.; Luo, J. B.; Erdemir, Ali. Influence of Tribofilm on Superlubricity of Highly-Hydrogenated Amorphous Carbon Films in Inert Gaseous Environments. *Sci. China: Technol. Sci.* **2016**, *59*, 1795−1803.
(48) Fontaine, J.; Le Mogne, T.; Loubet, J.; Belin, M. Achieving Superlow Friction with Hydrogenated Amorphous Carbon: some Key Requirements. *Thin Solid Films* **2005**, *482*, 99−108.

https://doi.org/10.1021/acsomega.1c05105
ACS Omega 2022, 7, 7472−7480